A&A, 696, A75 (2025)
https://doi.org/10.1051/0004-6361/202453557

Astronomy & Astrophysics

Jets downstream of the Martian bow shock

Occurrence in the 2014–2024 period

Tara Mohammed-Amin[1,2,⋆], Eva Krämer[1,⋆], Sara Nesbit-Östman[1,⋆], Herbert Gunell[1,⋆⋆], and Cyril Simon Wedlund[3]

[1] Department of Physics, Umeå University, 901 87 Umeå, Sweden
[2] HiQ, Stockholm, Sweden
[3] Austrian Academy of Sciences, Space Research Institute, 8042 Graz, Austria

Received 20 December 2024 / Accepted 5 March 2025

ABSTRACT

Context. Dynamic pressure enhancements, known as magnetosheath jets, are plasma structures with a higher dynamic pressure than the surrounding plasma. They have been thoroughly studied at Earth and recently discovered around other planetary bodies. However, studies on jets outside of the terrestrial magnetosheath have only been performed as case studies.
Aims. We present the first statistical study of jets in the Martian plasma environment.
Methods. Our database was assembled using ten years of Mars Atmosphere and Volatile Evolution (MAVEN) mission data sampling various regions in the Martian plasma environment.
Results. Our database contains 82 645 jets, which have an average dynamic pressure increase of a factor of 2.34. The majority of jets are observed close to the bow shock in the magnetosheath. Most jets are driven by a combination of velocity and density enhancement, although the distribution is skewed toward density enhancement, as compared to jets at Earth. The jets are often colder than their background. The median scale size of Martian jets is 0.67 R_M.
Conclusions. Jets in the Martian plasma environment are similar to jets observed in the terrestrial magnetosheath, however, there are some differences. In Martian jets, the density enhancement dominates over the velocity; whereas in terrestrial jets, the velocity enhancement dominates over the density enhancement. Furthermore, jets are more deflected compared to the surrounding magnetosheath plasma. Martian jets are likely to be smaller than terrestrial jets, but they are larger relative to the scale size of the magnetosphere.

Key words. plasmas – methods: data analysis – planets and satellites: individual: Mars

1. Introduction

Bow shocks are a universal phenomenon in space plasmas, which act to compress, slow down, and heat the incoming plasma. They give rise to magnetosheath jets, which are transient dynamic pressure enhancements that have been intensely studied in the near-Earth plasma environment (Plaschke et al. 2018; Krämer et al. 2025). Recently, jets have also been found in other planetary environments such as Mars (Gunell et al. 2023), Jupiter (Zhou et al. 2024), and downstream of planetary shocks (Hietala et al. 2024). These studies have only presented a few jets, such that the properties and statistics of magnetosheath jets in other plasma environments still remain largely unexplored. Thankfully, the Mars Atmosphere and Volatile Evolution (MAVEN; Jakosky et al. 2015) spacecraft has been in orbit around Mars for ten years and offers a full suite of plasma instruments. We used these ten years of MAVEN data to conduct a statistical study of jets in the Martian plasma environment to understand similarities and differences of these jets compared to jets in the terrestrial magnetosheath.

Magnetosheath jets were first described by Němeček et al. (1998) in the Earth's magnetosheath and have since been studied extensively (see Plaschke et al. 2018; Krämer et al. 2025, and references therein). The presence of solar wind monitors has enabled detailed studies of jet formation depending on solar wind conditions. Such works have reported that it is primarily controlled by the angle between the interplanetary magnetic field (IMF) and the bow shock normal, θ_{Bn} (Archer & Horbury 2013; Plaschke et al. 2013; LaMoury et al. 2021). Jet detection rate increases during times of low θ_{Bn}. Nevertheless, Goncharov et al. (2020) showed that jets can also be frequently observed downstream of the bow shock during high θ_{Bn}.

The driver of a jet can be an enhancement in velocity, density, or a combination of both. Archer & Horbury (2013) found that 82% of jets exhibit both a density and a velocity increase, while 18% of jets show an increase in velocity, but with a decrease in density. In addition, the majority of jets were found to show changes in the magnetosheath's magnetic field. Furthermore, the temperatures have been found to be more isotropic and lower compared to the surrounding magnetosheath plasma (Plaschke et al. 2013). The scale size of the magnetosheath at Earth is of the order of 0.1 R_E and the distribution are expected to follow a log-normal distribution, according to Plaschke et al. (2020). Nonetheless, jets with sizes >2 R_E are also commonly observed, causing eight jet impacts per hour on the subsolar magnetopause during low θ_{Bn} conditions (Plaschke et al. 2020).

The solar wind environment at Mars is in many ways similar to that at Earth. The median value for the solar wind velocity is 400 km/s, with a density typically in the range 0.5–20 cm^{-3} (Halekas 2017). The IMF has a magnitude that is typically in the range of 0.5–10 nT and a median cone angle of 61° from the Mars-Sun line (Halekas et al. 2021).

⋆ These authors contributed equally to this work.
⋆⋆ Corresponding author; herbert@herbertgunell.se

Bow shocks have regions of quasi-parallel and quasi-perpendicular alignments, where θ_{bn} is $0° < \theta_{bn} < 45°$ and $45° < \theta_{bn} < 90°$, respectively (e.g. Greenstadt et al. 1970). Due to the induced nature of the Martian system, the Martian magnetosphere is small compared to Earth. A typical Martian subsolar bow shock stand-off distance is ~1.6 R_M, with one Mars radius of R_M = 3390 km. The induced magnetopause boundary (IMB) is typically measured to be at a distance of ~1.3 R_M (Vignes et al. 2000).

Between these two boundaries lies the magnetosheath, where the plasma is compressed and heated, and the flow is decelerated and deflected. Given the bow shock and IMB distances from Vignes et al. (2000), the average subsolar magnetosheath width becomes 0.3 R_M (~1017 km). Due to the small scale of the magnetosheath compared to ion scales, the flow does not have time to fully thermalize in the magnetosheath (Moses et al. 1988). Typical Martian magnetosheath parameters are a flow velocity of 100–200 km/s and an ion density of 10 cm^{-3} (Halekas et al. 2017). Following the upstream bow shock geometry, the magnetosheath can be divided into quasi-perpendicular and quasi-parallel magnetosheath, where the quasi-parallel magnetosheath is typically more turbulent (Fuselier 1994; Karlsson et al. 2021).

Jets in the Martian magnetosheath were first presented by Gunell et al. (2023), using data from the MAVEN mission. The jets had a duration of 30−60 s which corresponds to a scale length of 4000−18 000 km. Gunell et al. (2023) also noted that this is in most cases more than the planetocentric distance to the bow shock and therefore indicates that jets are beams that are continuously generated at the bow shock. In addition, the authors showed that the plasma inside jets have larger magnetic field fluctuations compared to the surrounding magnetosheath.

Jets in the Jovian magnetosheath were first described by Zhou et al. (2024). The authors studied three jets which were found to last between ten minutes and up to an hour. Through a comparison of the jet sizes at Earth, Mars, and Jupiter, Zhou et al. (2024) suggested that the size of the jets scales with the size of the bow shock.

Although jets have been found in the Martian magnetosheath, Jovian magnetosheath, and downstream of interplanetary shocks, those jets have only been presented as case studies in the past. We present the first statistical study of jets outside Earth. With this study, we aim to infer the behavior of jets at Mars and how they scale in the Martian plasma environment compared to Earth. We investigate their occurrence rate, their properties, and what quantity drives the pressure density enhancement. The paper is structured as follows. In Sect. 2, we describe the methods used to build our database for magnetosheath jets at Mars. In Sect. 3, we present the statistical properties of jets found at Mars, along with a discussion of our findings and a comparison with findings at Earth. Finally, our conclusions are given in Sect. 4.

2. Instrumentation and methods

The data used in this study come from the MAVEN mission (Jakosky et al. 2015) over the period October 2014–January 2024. For our statistical study on jets, data from two instruments were used. The first instrument was the Solar Wind Ion Analyzer (SWIA; Halekas et al. 2015), a top-hat electrostatic analyzer that measures protons in the solar wind and magnetosheath from which the proton moments are calculated. It has a temporal resolution of 4–8 s and a 360° × 90° field of view. Although the coarse archive mode data (SWICA) is the most accurate mode in the magnetosheath, we chose to use the on-board calculated moments at the highest available resolution, assuming that the plasma is mainly composed of protons H^+. We checked that the two modes were in good agreement throughout (see Halekas et al. 2017, for further discussion). The second instrument was the magnetometer (MAG; Connerney et al. 2015), which measures the vector magnetic field at a frequency of 32 Hz. The Mars-centered Solar Orbital (MSO) coordinate system is used throughout the study. It has its origin at the center of Mars, $\hat{x}$, pointing toward the Sun, $\hat{y}$, pointing in the negative orbital direction of Mars, and $\hat{z}$ completing the right-hand system.

We wanted to look at jets behind the bow shock and above the IMB. Jets were detected in the region defined by the following constraints:

1. We required the telemetry mode flag to indicate that SWIA was in its magnetosheath mode.
2. We required the spacecraft to be located inside a bow shock model by Ramstad et al. (2017) with a solar wind density of n_{sw} = 2 cm^{-3} and solar wind speed of v_{sw} = 400 km s^{-1} as the input parameters.
3. At the inner boundary, the values taken below 1000 km above the planet's surface and in the shadow of the planet were discarded. The shadow was defined as a cylinder, where $x_{MSO} < 0$ with a radius of R_M+1000 km.

To create a common timebase for all quantities, we low-pass-filtered and down-sampled the magnetic field data to a time series with a 1 Hz sampling frequency. The time frame was adjusted, so that the samples in the new time series would be as close as possible to the time stamps of the SWIA moment data. An equally sampled time series was created from the SWIA moments, using linear interpolation. These 1 s sampling-interval time series were used throughout the study.

For a jet detection, we compared the local dynamic pressure $P_{dyn} = m_p n_i v_i^2$ with the background dynamic pressure. Here, m_p is the proton mass, and n_i and v_i are the ion density and bulk speed, respectively, as measured by SWIA. We use the same criteria as Gunell et al. (2023), which is similar to the criterion used by Archer et al. (2012). We calculated a ten-minute moving average centered at the dynamic pressure around the time stamp, denoted $\langle P_{dyn} \rangle_{10\,min}$. If any part of the ten-minute interval fell outside of the region of interest, which happens when the spacecraft moves into or out of that region, the first or last complete ten-minute interval on the inside was used instead. We discarded the jet indications for data points within 8 seconds from a flagged field-of-view problem or a flag indicating that the attenuators or telemetry mode were in an ambiguous state. When the data quality was good, the jet events needed to satisfy

$$P_{dyn} > 2\langle P_{dyn} \rangle_{10\,min}. \quad (1)$$

Furthermore, we present statistics on the dynamic pressure, density, velocity components, magnetic field strength, and temperature of the jet. In addition, we investigate the scale size of the jets, estimated by $D = t \cdot |\mathbf{v}|$, where t is the duration of the jet and $\mathbf{v}$ is the mean velocity of the jet. We also present the ratio of the maximum value of these properties in the jets to the average background values. The background values were calculated in the same way as $\langle P_{dyn} \rangle$ was calculated: by taking a ten-minute moving average. This background includes the jet observation.

In order to investigate if jets are mainly density- or velocity-driven, we used the approach described by Archer & Horbury (2013) and established:

$$\rho = \langle \rho \rangle + \Delta\rho, \quad (2)$$

$$v^2 = \langle v^2 \rangle + \Delta(v^2), \tag{3}$$

where the angled brackets denote the background value and delta some deviation. This can be approximated as

$$1 \simeq \frac{\Delta n / \langle n \rangle}{\Delta P_{\rm dyn} / \langle P_{\rm dyn} \rangle} + \frac{\Delta(v^2) / \langle v^2 \rangle}{\Delta P_{\rm dyn} / \langle P_{\rm dyn} \rangle} + \frac{(\Delta n / \langle n \rangle)(\Delta(v^2) / \langle v^2 \rangle)}{\Delta P_{\rm dyn} / \langle P_{\rm dyn} \rangle}, \tag{4}$$

using the approximation $\langle P_{\rm dyn} \rangle = \langle n \rangle \langle v^2 \rangle$ (Archer & Horbury 2013). Determining the first two terms for every jet reveals which one is the dominant term and how much each quantity contributes to the dynamic pressure enhancement. The final term reveals how the different components contribute to a jet and is assumed to be small. Plotting the two first terms against each other illustrates how dominant they are per jet.

We also studied the ion temperature variations and the temperature anisotropy in the jets. The ion temperatures and their components parallel and perpendicular to the local magnetic field are calculated using the analytical method described by Swisdak (2016, see their Appendix A) and checked against the matrix method of Simon Wedlund et al. (2022, see their Appendix B.2). The symmetric rank-2 ion (i.e. proton) thermal pressure tensor, denoted $\mathbb{P}_{x,y,z}$, is first constructed from the on-board moments of the ion distribution function from SWIA data. The analytical expression takes advantage of the principal invariants of the pressure tensor to obtain the $P_{\parallel}$ component as:

$$P_{\parallel} = P_{xx} b_x^2 + P_{yy} b_y^2 + P_{zz} b_z^2 + 2\left(P_{xy} b_x b_y + P_{xz} b_x b_z + P_{yz} b_y b_z\right), \tag{5}$$

with $\mathbf{b} = \left(b_x, b_y, b_z\right)$ as the local normalised magnetic field vector in the chosen frame of reference. The $P_{\perp}$ component is finally derived from:

$$P_{\perp} = \frac{1}{2}\left(\mathrm{Tr}\, \mathbb{P}_{x,y,z} - P_{\parallel}\right), \tag{6}$$

where $\mathrm{Tr}\, \mathbb{P}_{x,y,z} = P_{xx} + P_{yy} + P_{zz}$ is the trace of the pressure tensor, which is invariant in any coordinate system. The ion temperature is simply obtained from the thermal pressure as $T = P/nk_B$, with k_B the Boltzmann constant, and with the total temperature, defined as $T_{\rm tot} = \mathrm{Tr}\, \mathbb{P}_{x,y,z}/3 = (T_{\parallel} + 2T_{\perp})/3$.

3. Results and discussion

In this section, we discuss the statistical properties of our jet database, which contains 82 645 jets in total. In particular, we focus on the magnetic field properties and plasma moments. For the plasma moments and magnetic field, we used the value X observed at the peak dynamic pressure of the jet. The background of the jet is denoted by $\langle X \rangle$. We also computed the ratio of the two quantities, denoted by $X/\langle X \rangle$. We also provide the median and mean for each quantity inside the jet in this work.

For comparison, we investigated a subset of jets in our database, namely, jets in the dayside magnetosheath ($x_{MSO} > 0$). We found 20 591 jets in the dayside magnetosheath. This subset of jets has been investigated, as statistical studies on jets in the Earth's magnetosheath are traditionally focused on either the subsolar magnetosheath or the dayside region (Plaschke et al. 2013; Archer & Horbury 2013; Goncharov et al. 2020; Raptis et al. 2020). The statistics of the subset are presented in Appendix A for dayside jets. In general, the statistics of the entire dataset and the subset are in agreement, with differences are discussed when relevant. We do not present statistics for the subsolar magnetosheath because of the poor data quality in this region.

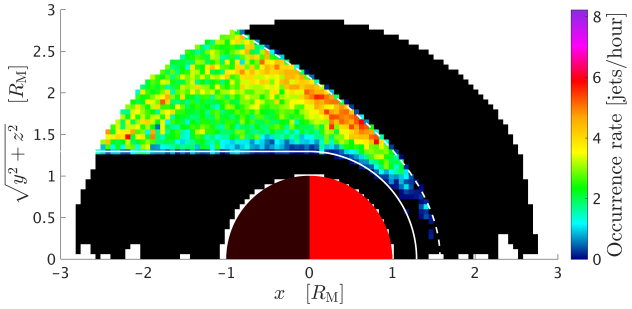

Fig. 1. Occurrence rate of jets in the cylindrical coordinates. The solid white line represents the inner boundary of our dataset. The dashed white line represents the outer boundary, i.e. the average bow shock position.

3.1. Occurrence

The probability of observing a jet at a certain position in the Martian plasma environment is given in Fig. 1 in cylindrical coordinates. To get the probability of a jet being found at a particular location, we divide the total duration a jet has been detected at that location by the total duration the spacecraft has passed there. As seen, most jets are observed on the flanks of the magnetosheath close to the bow shock. Of the 82 645 jets, 20 591 were observed on the dayside ($x_{\rm MSO} > 0$). There are only a few jets observed in the Martian subsolar magnetosheath and the occurrence rate increases for $\sqrt{y^2 + z^2} > 1\ R_{\rm M}$. The increased occurrence rate of jets close to the bow shock is in agreement with observations at Earth (Plaschke et al. 2013). Those jets are likely formed at the bow shock (Hietala & Plaschke 2013; Raptis et al. 2022; Suni et al. 2021) and move through the magnetosheath, where they interact with the ambient plasma and dissipate.

On Earth, jets are frequently reported in the subsolar magnetosheath (Plaschke et al. 2013), however, such jets are missing in Fig. 1. Our database is biased due to the field-of-view quality flag. Because the bulk plasma flow is outside the field of view of the SWIA instrument, jets in the subsolar magnetosheath were excluded. However, in theory, fewer jets are expected in the Martian subsolar magnetosheath than in the corresponding region near Earth. One factor is that the Parker spiral at Mars is 61° (Halekas et al. 2021), which means that there are fewer occurrences of a quasi-parallel bow shock in the subsolar region. In turn, this leads to fewer jet formations, as the occurrence of jets is strongly coupled to the quasi-parallel bow shock (Vuorinen et al. 2019).

Another factor that might control the occurrence rate of jets are very low cone angles. Fowler et al. (2022) suggested that for very low cone angles, the Martian environment becomes highly dynamic and the solar wind is not fully deflected around the planet. Instead, they observed a foreshock-like plasma in a region that usually constitutes the magnetosheath. Further evidence was provided by Zhang et al. (2024), who showed that at very low cone angles, the Martian bow shock degenerates. Since the bow shock dynamics are of different nature in these

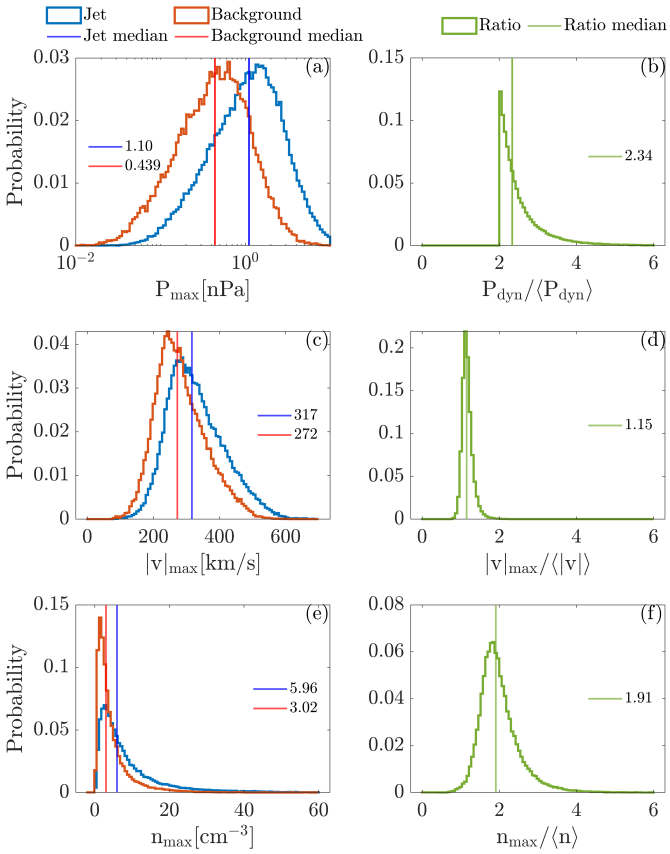

Fig. 2. Distributions of dynamic pressure, bulk velocity, and number density. The left column shows the distributions of these quantities for the jets and for the background. The jet values represent the maximum value measured inside the jet. In the right column the ratio between the maximum and the background averages is shown. The vertical lines show the median values.

quasi-parallel conditions, the question remains as to how this affects jet formation.

The occurrence rate of jets increases in the magnetotail lobes, where $\sqrt{y^2+z^2} < 2\ R_M$ and $x \approx 2\ R_M$. The cluster in the lobes is in a region where both the jet occurrence rate (see Fig. B.1) and the time spent by the MAVEN spacecraft in this region are low (less than 1 day per bin; see Fig. B.2). This might cause the occurrence rate in some bins to be large due to low statistics. However, since the total number of jet observations is low in this region, those jets are not well represented in our database. Most of the jets in our database are found close to the bow shock.

3.2. Dynamic pressure

In the left column of Fig. 2, we see the distribution of the maximum values of dynamic pressure P_{max} in a jet (Fig. 2a), and the values of the ion velocity v_{max} (Fig. 2c), and density n_{max} (Fig. 2e), at the time of maximum dynamic pressure. In the right column, we see the ratio between the same quantities and the averages of the surrounding magnetosheath (Figs. 2b, d, and f). In Fig. 2a, the distribution of the maximum dynamic pressure is plotted. The median of the jet distribution is 1.10 nPa. The distributions of P_{max} of the jets (blue) and of the background magnetosheath (red) are similar, with the exception of the jet distribution being shifted toward higher values. In Fig. 2b, we

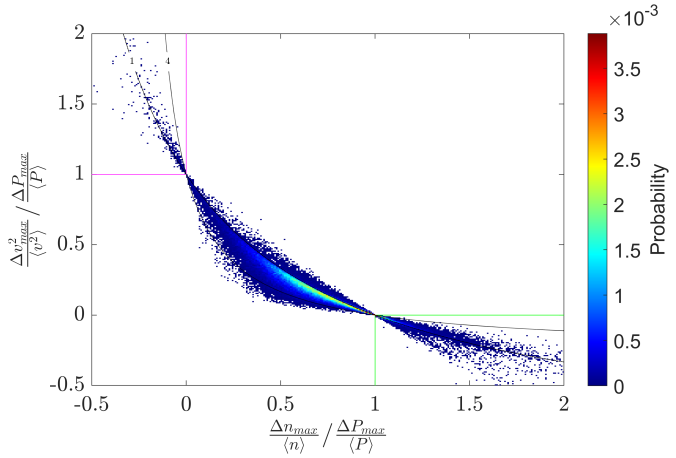

Fig. 3. Density-driven vs velocity-driven jets at Mars. The pink box encapsulates jets completely driven by velocity enhancements, the green box encapsulates jets completely driven by density enhancements. The lines display contours of $\Delta P_{max}/\langle P\rangle$.

see the ratio of the maximum P_{max} and the surrounding magnetosheath average. The majority of the distribution is in the 2–4 interval, with the median value being 2.34. The cut-off at 2 is due to the definition of jets as $P_{dyn} > 2\langle P_{dyn}\rangle_{10\,min}$.

This is slightly lower than that found on Earth. Plaschke et al. (2013) plotted the inverse ratio and found the peak of their distribution around 0.2–0.3, which corresponds to a ratio of 3.33–5 using the same ratio as in this study. However, Plaschke et al. (2013) used only the dynamic pressure in the x-direction, which is the largest component of P_{dyn} (see velocity components of the jets in Fig. 4), which makes a direct comparison more difficult.

In Fig. 2c, the distribution of $|v_{max}|$ observed in the jets is shown. The distribution is centered around 270 km/s, with the minimum and maximum found around 100 and 600 km/s, respectively. The median value is 317 km/s. Figure 2d shows the ratio between v_{max} and the average velocity of the surrounding magnetosheath. The distribution is narrow, with most jets falling in the 1–2 interval and with a median value of 1.15. In Fig. 2e the distribution of the maximum density observed in the jets is shown. Most jets have a density in the range 0–20 cm^{-3}, but values as high as 60 cm^{-3} are observed. The median value for jets is 5.96 cm^{-3}. In Fig. 2f, the ratio between n_{max} and the average density of the surrounding magnetosheath is shown. The majority of the distribution is in the 1–4 interval, with the median ratio being 1.91. This is larger than the velocity ratio (even taking into consideration that the velocity is squared in the expression for the dynamic pressure), showing that the density on average contributes more to the dynamic pressure enhancement.

We further investigated the major driver of the jet, using the first two terms of Eq. (4). The result is given in Fig. 3, which illustrates the distribution of jets in the density-velocity parameter space. Jets in the pink box have an increase in velocity and a decrease in density compared to the background magnetosheath. The jets in the green box have reversed characteristics, with a decrease in velocity and an increase in density. The vast majority of the distribution is between these two categories, with the dynamic pressure enhancement arising from an increase in both velocity and density. The distribution peaks with a larger contribution from the density, at [0.7, 0.25]. From the distribution, we can see that purely velocity-driven jets are rare. At Earth, Archer & Horbury (2013) found that 18% of the jets were driven solely by velocity, 82% were driven by increases in both velocity

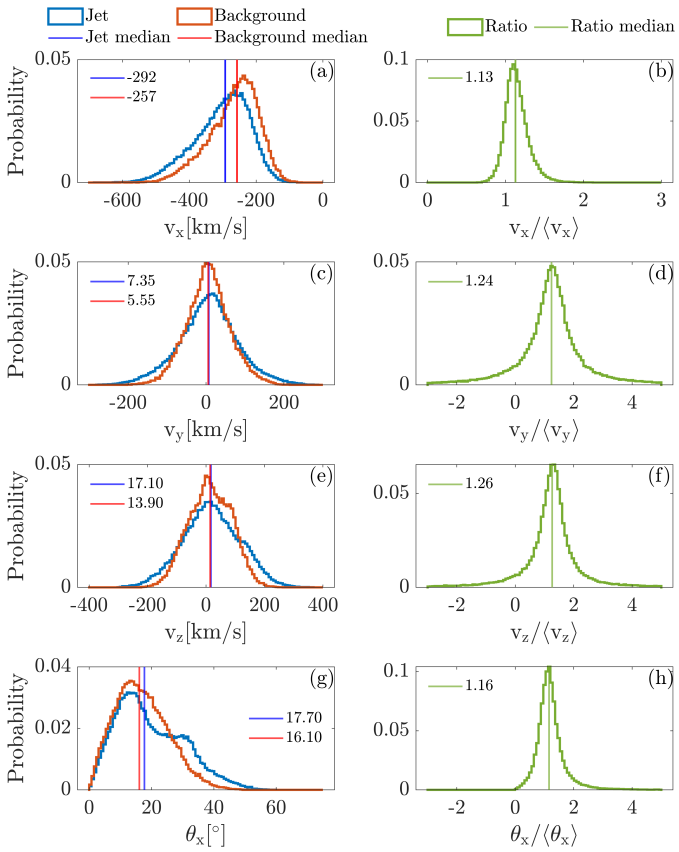

Fig. 4. Distributions of the velocity components, $v_{x,y,z}$, and the deflection angle, θ_x. The left column shows the distributions of these quantities for the jets and for the background. The jet values represent the maximum value measured inside the jet. In the right column, the ratio between the maximum and the background averages is shown. The vertical lines show the median values.

and density, and very few by increases in density alone. Their distribution peaked closer to [0.2 0.5], showing a lesser contribution from increases in density and showing that most jets were velocity-driven. This therefore differs from our results, with jets at Earth in general being more velocity-driven, compared to jets at Mars. However, Raptis et al. (2020) found that fewer than 0.5% of the jets found in the quasi-parallel magnetosheath (quasi-parallel jets) were solely velocity-driven, which reflects a greater similarity to our findings. Our Martian jets therefore most resemble quasi-parallel jets at Earth in this aspect. Figure A.2 shows the same graph but contains only the dayside jets of our dataset. The distribution is largely similar to that in Fig. 3, showing that the driving properties of the jets are similar for the whole dataset, regardless of where in the magnetosheath they are found.

3.3. Velocity components and deflection angle, θ_x

Figure 4 shows the distribution of the velocity components $v_{x,y,z}$ at the time of the dynamic pressure peak during each jet observation (Figs. 4a, c, and e) as well as the deflection angle $\theta_x = \cos^{-1}(v_x/|v|)$ of the velocity from the Earth–Mars line (Fig. 4g). The figure also shows the ratio of the velocity components and the deflection angle compared to the background (Figs. 4b, d, f, and h). The same figure was produced for jets on the Martian dayside (Fig. A.3).

All jets move in the anti-sunward direction (v_x<0; Fig. 4a). The median velocity along x is −292 km/s. This ratio $v_x/\langle v_x\rangle$ is between 1 and 2, indicating that v_x is usually increased in jets compared to the surrounding magnetosheath (Fig. 4b). The median value is 1.13, which indicates that v_x is not solely responsible for the detection of jets, as this would require an increase of $\sqrt{2} = 1.41$, seen from Equation (3).

Figure 4c shows the distribution of v_y which is approximately centered around 0 km/s with median values of 7 km/s. The median of $v_y/\langle v_y\rangle$ is 1.24 (Fig. 4d). We can conclude that jets often experience an increase in v_y, which is stronger than the increase in v_x. This indicates that jets can be more deflected than the background magnetosheath plasma.

The distribution of v_z, which is also centered around 0 km/s, is plotted in Fig. 4e. The median value is 17 km/s. The ratio $v_z/\langle v_z\rangle$ (Fig. 4f) peaks at 1.26 (median value), which is similar to the increase in v_y. The v_z distribution is wider than the v_y distribution due to orbital effects. The MAVEN spacecraft has a highly elliptical polar orbit. On average, v_z is therefore increased at the flanks when the plasma is deflected around the planet. This becomes more evident in Fig. A.3e, where v_z exhibits a double peak due to that effect, while v_y lacks such a double peak. Both distributions, v_y and v_z, are broader compared to their background distribution indicating a higher variability in the velocity.

To better assess how the propagation of jets changes compared to the surrounding magnetosheath, we also investigated the change in the deflection angle, θ_x (see Fig. 4g). The median of the deflection angle ratio is 1.2, which is similar to values seen on the dayside (see Fig. A.3g). This stands in contrast to the findings of Plaschke et al. (2013) who found a smaller deflection angle of jets compared to plasma preceding the jet. Also, Raptis et al. (2020) found that quasi-parallel jets at Earth are less deflected, while jets in the quasi-perpendicular magnetosheath (quasi-perpendicular jets) have larger deflection angles. In this aspect, the Martian jets are more similar to quasi-perpendicular jets at Earth.

The distribution of the deflection angle for jets shows two peaks, one at 15° and one at 35°, while the background distribution only has one peak. Figure 4h shows the ratio again and indicates that jets tend to have a larger deflection angle compared to the magnetosheath. From the deflection angle of jets in the dayside magnetosheath (Fig. A.3g) it becomes evident that the large deflection angle stems from the deflection of the plasma around the planet. Interestingly, the average deflection angle for quasi-parallel jets is 34.8° (Raptis et al. 2020), which is similar to the second peak at 35° representing dayside jets. This indicates that the deflection angle of Martian jets resembles quasi-parallel jets on Earth.

In summary, jets show a relative increase in all velocity components, but predominantly in v_y and v_z and less in v_x. We also find that jets have a larger deflection angle compared to the surrounding magnetosheath, in contrast to previous studies in the Earth's dayside magnetosheath. Meanwhile, the absolute deflection angle for dayside jets is similar to the deflection angle found for quasi-parallel jets at Earth.

3.4. Temperature

Figure 5 shows the temperature of the jets, with Fig. 5a showing the distribution of the ratio $T_\perp/T_\parallel$ for both the jets and the background. We can see that the temperature is largely isotropic, with both of the distributions centered around 1, and with medians of 1.04 and 1.01 for the jets and background, respectively.

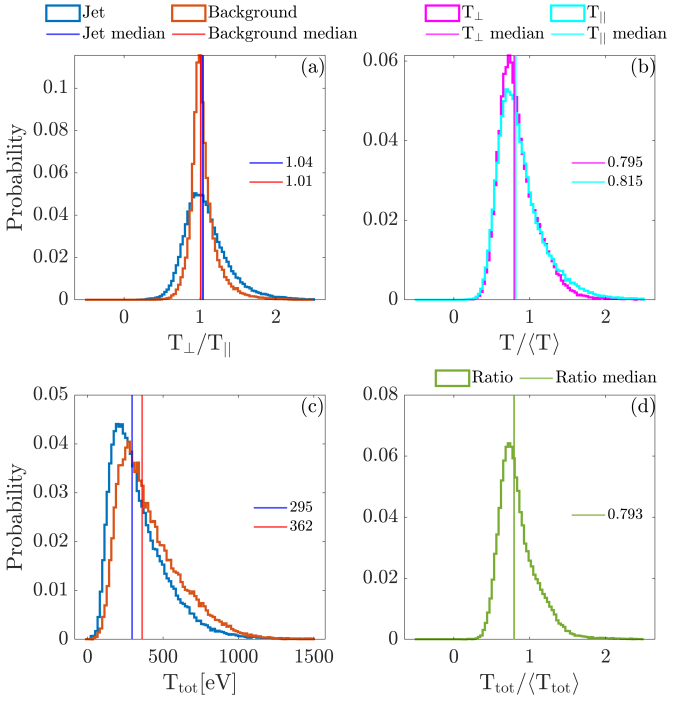

Fig. 5. Distributions of ion temperature. The graphs show the following: (a) the ratio $T_\perp/T_\parallel$ for the jets and the background, (b) the ratio of the jet maximum to the background for components $T_\perp$ and $T_\parallel$, (c) the distribution functions for the jet maximums and the background, and (d) the ratio of the jet maximum to the background for the total temperature. The vertical lines signify the medians of the distributions.

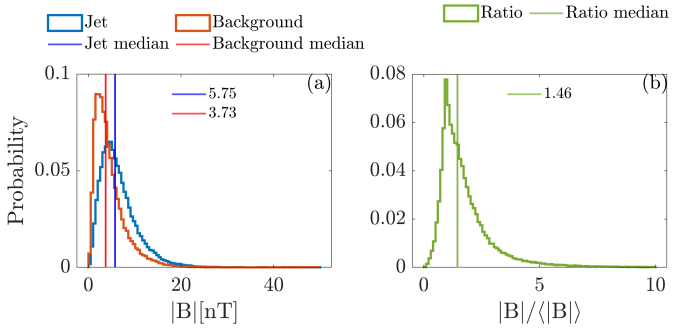

Fig. 6. Distributions of the total magnetic field $|B|$. The graphs show the following: (a) distributions of the maximum magnetic field measured in the jet and the background and (b) the ratio of the maximum value inside the jets to the background. The vertical lines signify the medians.

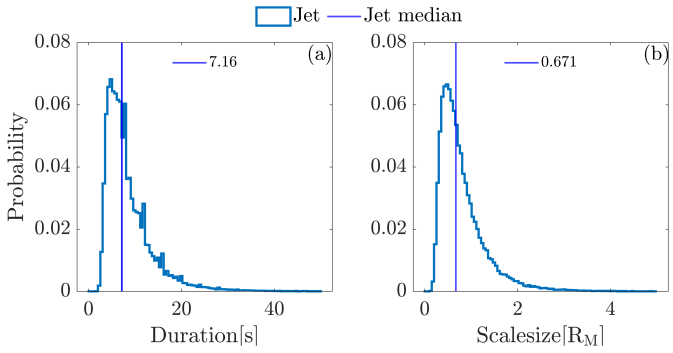

Fig. 7. Distribution of the jet duration in (a) and the distribution of the jet scale size in (b).

The jet distribution is slightly broader than that of the background, indicating a slightly larger temperature anisotropy inside the jets, compared to that of the background. These results are also reflected in Fig. 5b, which shows the ratio of the jet maximum temperature to the background mean temperature, for $T_\perp$ and $T_\parallel$. The distributions are very similar, with only a slight broadening of the parallel temperature ratio. For terrestrial magnetosheath jets, Plaschke et al. (2013) found that $T_\perp$ is often enhanced over $T_\parallel$, but the temperature in jets is more isotropic compared to the surrounding magnetosheath. Plaschke et al. (2013) also found that the temperature anisotropy prior to the jet observation is decreased, which could explain our isotropic background measurements. Raptis et al. (2020) found that quasi-parallel jets on average have less of an ion temperature anisotropy than quasi-perpendicular jets, as is the case of the quasi-parallel magnetosheath on Earth (Dimmock et al. 2015; Karlsson et al. 2021). The low ion temperature anisotropy of our Martian jets is therefore similar to quasi-parallel jets on Earth.

In Fig. 5c, we see the total temperature distribution for the jets and the background. Jets are generally colder than the background from the shift in the distributions. This result is also reflected in Fig. 5d, which shows the ratio of the maximum jet temperature over the background. The median value is 0.758, showing that the jets are generally colder than the surrounding plasma. This is similar to what has been observed at Earth, where Plaschke et al. (2013) found that the jets on average were colder than the background. Furthermore, Raptis et al. (2020) found the same for quasi-parallel jets and boundary jets (jets at the boundary between the quasi-parallel and quasi-perpendicular magnetosheath), but not for quasi-perpendicular jets. Colder temperatures in jets support the theory of jets being generated at the bow shock, as it is an indicator that the jets contain solar wind plasma that is less decelerated and heated compared to the surrounding plasma.

3.5. Magnetic field

The distribution of the total magnetic field, $|B|$, and the corresponding ratio, $|B|/\langle B\rangle$, are given in Fig. 6. The median magnetic field is 5.8 nT and it is stronger inside the jets, compared to the background. The median ratio is 1.46 for the magnetic field. An increase in the magnetic field inside jets compared to the background was also reported in terrestrial jets (Plaschke et al. 2013) and for quasi-parallel and boundary terrestrial jets by Raptis et al. (2020).

The magnetic field in jets on the dayside is higher, with a median of 8.05 nT (Fig. A.5a). This is likely related to the stronger magnetic field pile-up downstream of the bow shock on the dayside.

3.6. Duration and size

Finally, we investigated the distribution of the jets' durations (Fig. 7a) and scale sizes (Fig. 7b). The duration varies between 4 − 30 s, with a median duration of 7.1 s (Fig. 7a). The median scale size is 0.67 R_M. This corresponds to 11 proton gyroradii, given an average proton gyroradius in the magnetosheath of 200 km, calculated from T_i = 100 eV, v_{th} = 140 km/s, and B = 7 nT. The scale size and duration on the dayside (Fig. A.6) are about 20% smaller, compared to the overall scale and duration.

The scale size distribution is biased towards larger jets, as it is more likely to observe large jets compared to small jets (Plaschke et al. 2020). The true median size of Martian jets

should therefore be smaller. On Earth, Plaschke et al. (2020) reported observed (biased) scale sizes of 0.89 R_E and 0.68 R_E in the perpendicular and parallel directions, respectively. Considering that 1 $R_M \approx 0.5\,R_E$, Martian jets have a smaller scale size, compared to terrestrial jets. As the Martian plasma environment is much smaller, there is no one-to-one relation on the size of the bow shock and the size of the resulting jets. Plaschke et al. (2020) found that the unbiased scale size for terrestrial jets is of the order of 0.1 R_E. We therefore suggest that the true, unbiased scale size of Martian jets is smaller and, furthermore, it is likely to be smaller than those on Earth as well.

The time resolution for the ion data is 4 s, which resolves jets of the order of 1200 km $\approx 0.4\,R_M$ (using $v = 300$ km/s). The detection of jets of smaller size can therefore not be guaranteed with the instrumentation on board the MAVEN spacecraft. If the peak dynamic pressure coincides with a suitable part of the SWIA scanning cycle, a jet could be detected, but there is a notable risk of missing such short jets. We previously argued that the unbiased scale size of Martian jets is likely to be lower than $0.1\,R_E \approx 0.2\,R_M$; however, jets of this size cannot be resolved with the instruments on MAVEN. This introduces a bias to our database in favor of larger jets.

The observed size of jets is only weakly depending on the region where they are observed even though the Martian magnetosheath is significantly thinner (0.3 R_M in the subsolar region), compared to Earth's magnetosheath, which has a thickness of several Earth radii . The average scale size is larger than the subsolar Martian magnetosheath, so jets produced at the bow shock could potentially reach the IMB. The jets observed by Gunell et al. (2023) had scale sizes of 4000−18 000 km (larger than 1 R_M). We find that these scale sizes are not representative of jets in the Martian magnetosheath.

4. Conclusion

We presented the first statistical study on dynamic pressure enhancements in the Martian plasma environment. The majority of jets were observed close to the bow shock in the magnetosheath, similar to magnetosheath jets observed in the terrestrial magnetosheath. This supports the idea that jets form at the bow shock and dissipate through interaction with the ambient magnetosheath plasma as they move through the magnetosheath.

Compared to terrestrial magnetosheath jets, the Martian jets exhibit very similar properties. Jets are mostly driven by increases in both density and velocity, the magnetic field is enhanced, and the temperature is decreased. However, Martian jets are (on average) more density-driven and the temperature is more isotropic, both inside the jets and the background, compared to Earth.

We found a median scale size of 0.67 R_M, which is smaller than the scale sizes reported at Earth. However, with respect to the scale size of the magnetosphere and thickness of the magnetosheath, the jets are much larger compared to jets at Earth. Zhou et al. (2024) suggested that the size of jets scales with the stand-off distance of the bow shock. We find that Martian jets are indeed smaller, while the stand-off distance of the bow shock is smaller as well. Considering that a thinner magnetosheath will cause jets to propagate smaller distances because of breaking effects close to the IMB, the stand-off distance will likely play a role. However, the scaling between the stand-off distance is rather weak, considering that the jets are a factor of 2 smaller, but the magnetosheath is an order of magnitude thinner. Thus, there might be other controlling factors connected to the jet-generation mechanism of the bow shock. This is supported by the fact that jets might be continuously generated at the bow shock (Gunell et al. 2023). Various studies have connected bow shocks to foreshock structures (Suni et al. 2021). Other generation mechanisms include bow shock reformation (Raptis et al. 2022), which might have a different reoccurrence rate, and bow shock ripples (Hietala & Plaschke 2013), which might have different scale sizes at Mars. Furthermore, there are different generation mechanisms for jets downstream of the quasi-parallel and quasi-perpendicular bow shock. Those jets might also scale differently due to different generation mechanisms. However, because of the lack of an upstream solar wind monitor, we were unable to differentiate between those different classes of jets.

Overall, Martian jets share similarities with quasi-parallel jets on Earth. This could be due to characteristics of the Martian plasma environment: escaping exospheric particles generate ultra-low-frequency (ULF) waves (Romanelli et al. 2016; Liu et al. 2020), similarly to that seen at Earth's foreshock (Greenstadt et al. 1995). Furthermore, a heavy ion foreshock at Mars exists due to pickup ions (Yamauchi et al. 2015; Masunaga et al. 2016). This will also generate ULF waves. In turn, this could generate jets that share properties with quasi-parallel jets even at the quasi-perpendicular bow shock. In conclusion, the broader spectrum of upstream ULF wave activity at Mars could mean that jets are more influenced by foreshock dynamics, irrespective of θ_{bn}, making the jets at Mars overall more similar to quasi-parallel jets at Earth.

The Martian jets studied by Gunell et al. (2023) had a larger scale size and longer duration than the average jet in our database. Although Plaschke et al. (2013), and similarly Raptis et al. (2020), found that jets are less deflected compared to the background, we find a larger deflection angle for jets. However, Plaschke et al. (2013) focused on the subsolar terrestrial magnetosheath, while our database contains very few jets in this region.

Upcoming missions such as BepiColombo (Benkhoff et al. 2010), on its way to Mercury, and M-Matisse (Sanchez-Cano et al. 2022), intended to go to Mars and currently in Phase A study by the European Space Agency, offer exciting opportunities to continue studying magnetosheath jets. Those missions will provide opportunities to study jets in other planetary environments than Earth with measurements upstream and downstream of the bow shock. Additionally, the study of jets in the subsolar magnetosheath could be possible, which could reveal how jets affect an induced magnetosphere. Due to the lack of an intrinsic magnetic field, the interaction mechanisms with the magnetosphere (if there are any) would be different from terrestrial jets.

Acknowledgements. This work was supported by the Swedish National Space Agency contract 2023-00208. The work of CSW was funded by the Austrian Science Fund (FWF) 10.55776/P35954. All MAVEN data are publicly available through the Planetary Data System `https://pds-ppi.igpp.ucla.edu/mission/MAVEN/` (NASA 2023). The jet database is available at `https://doi.org/10.5281/zenodo.14215141`.

References

Archer, M. O., & Horbury, T. S. 2013, Ann. Geophys., 31, 319
Archer, M. O., Horbury, T. S., & Eastwood, J. P. 2012, J. Geophys. Res: Space Physics, 117, 5228
Benkhoff, J., Van Casteren, J., Hayakawa, H., et al. 2010, P&SS, 58, 2
Connerney, J., Espley, J., Lawton, P., et al. 2015, Space Sci. Rev., 195, 257
Dimmock, A., Osmane, A., Pulkkinen, T., & Nykyri, K. 2015, J. Geophys. Res. Space Phys., 120, 5489
Fowler, C. M., Hanley, K. G., McFadden, J., et al. 2022, J. Geophys. Res: Space Physics, 127, e2022JA030726

Fuselier, S. A. 1994, Geophys. Monogr. Ser., 81, 107
Goncharov, O., Gunell, H., Hamrin, M., & Chong, S. 2020, J. Geophys. Res: Space Physics, 125, e2019JA027667
Greenstadt, E., Green, I., & Inouye, G. 1970, Dual Satellite Observations of Earth's Bow Shock. III. Field-determined Shock Structure, Tech. rep., TRW Systems Group, Redondo Beach, California
Greenstadt, E., Le, G., & Strangeway, R. 1995, Adv. Space Res., 15, 71
Gunell, H., Hamrin, M., Nesbit-Östman, S., Krämer, E., & Nilsson, H. 2023, Sci. Adv., 9, eadg5703
Halekas, J. 2017, J. Geophys. Res: Planets, 122, 901
Halekas, J., Taylor, E., Dalton, G., et al. 2015, Space Sci. Rev., 195, 125
Halekas, J., Brain, D., Luhmann, J., et al. 2017, J. Geophys. Res: Space Phys., 122, 11
Halekas, J. S., Luhmann, J. G., Dubinin, E., & Ma, Y. 2021, Magnetospheres in the Solar System, 391
Hietala, H., & Plaschke, F. 2013, J. Geophys. Res., 118, 7237
Hietala, H., Trotta, D., Fedeli, A., et al. 2024, MNRAS, 531, 2415
Jakosky, B. M., Lin, R. P., Grebowsky, J. M., et al. 2015, Space Sci. Rev., 195, 3
Karlsson, T., Raptis, S., Trollvik, H., & Nilsson, H. 2021, J. Geophys. Res. Space Phys., 126, e2021JA029269
Krämer, E., Koller, F., Suni, J., et al. 2025, Space Sci. Rev., 221, 1
LaMoury, A. T., Hietala, H., Plaschke, F., Vuorinen, L., & Eastwood, J. P. 2021, J. Geophys. Res: Space Phys., 126, e2021JA029592
Liu, D., Yao, Z., Wei, Y., et al. 2020, Earth Planet. Phys., 4, 51
Masunaga, K., Seki, K., Brain, D., et al. 2016, J. Geophys. Res.: Space Phys., 121, 3093
Moses, S., Coroniti, F., & Scarf, F. 1988, Geophys. Res. Lett., 15, 429
NASA. 2023, Planetary Data System
Němeček, Z., Šafránková, J., Přech, L., et al. 1998, Geophys. Res. Lett., 25, 1273
Plaschke, F., Hietala, H., & Angelopoulos, V. 2013, Ann. Geophys., 31, 1877
Plaschke, F., Hietala, H., Archer, M., et al. 2018, Space Sci. Rev., 214, 81
Plaschke, F., Hietala, H., & Vörös, Z. 2020, J. Geophys. Res: Space Phys., 125, e2020JA027962
Ramstad, R., Barabash, S., Futaana, Y., & Mats Holmström, M. 2017, J. Geophys. Res. (Space Phys.), 122, 7279
Raptis, S., Karlsson, T., Plaschke, F., Kullen, A., & Lindqvist, P.-A. 2020, J. Geophys. Res: Space Physics, 125, e2019JA027754
Raptis, S., Karlsson, T., Vaivads, A., et al. 2022, Nat. Commun., 13, 598
Romanelli, N., Mazelle, C., Chaufray, J.-Y., et al. 2016, J. Geophys. Res.: Space Phys., 121, 11
Sanchez-Cano, B., Opgenoorth, H., Leblanc, F., Andrews, D., & Lester, M. 2022, 44th COSPAR Scientific Assembly, Held 16–24 July, 44, 421
Simon Wedlund, C., Volwerk, M., Beth, A., et al. 2022, J. Geophys. Res: Space Physics, 127, e2021JA029942
Suni, J., Palmroth, M., Turc, L., et al. 2021, Geophys. Res. Lett., 48, e2021GL095655
Swisdak, M. 2016, Geophys. Res. Lett., 43, 43
Vignes, D., Mazelle, C., Rme, H., et al. 2000, Geophys. Res. Lett., 27, 49
Vuorinen, L., Hietala, H., & Plaschke, F. 2019, Ann. Geophys., 37, 689
Yamauchi, M., Lundin, R., Frahm, R., et al. 2015, P&SS, 119, 48
Zhang, Q., Barabash, S., Holmstrom, M., et al. 2024, Nat., 1
Zhou, Y., Raptis, S., Wang, S., et al. 2024, Nat. Commun., 15, 4

Appendix A: Jets in the dayside magnetosheath of Mars

Here, we present the properties of jets in the dayside magnetosheath, that is, jet measurements where $x > 0$. The figures show the same quantities as Figs. 2–7. The only difference is that in this appendix only jets with $x > 0$ are included.

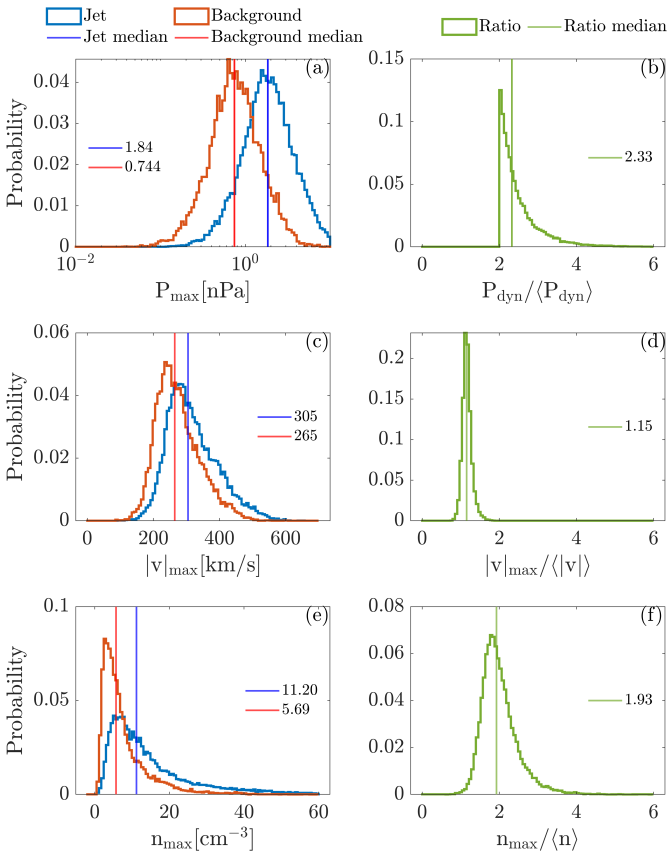

Fig. A.1. Same as Fig. 2, but for jets in the dayside magnetosheath.

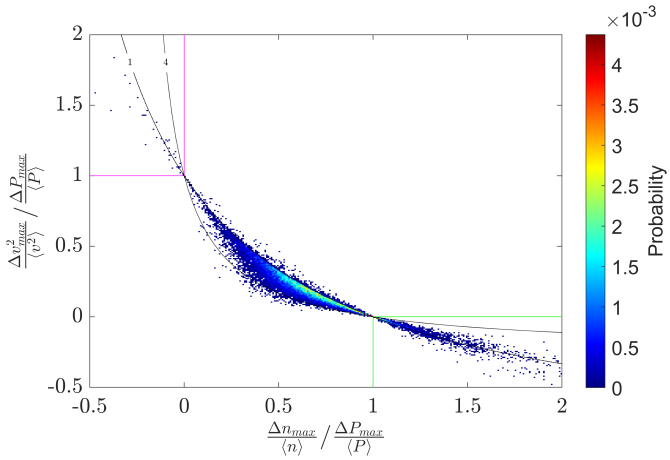

Fig. A.2. Same as Fig. 3, but for jets in the dayside magnetosheath.

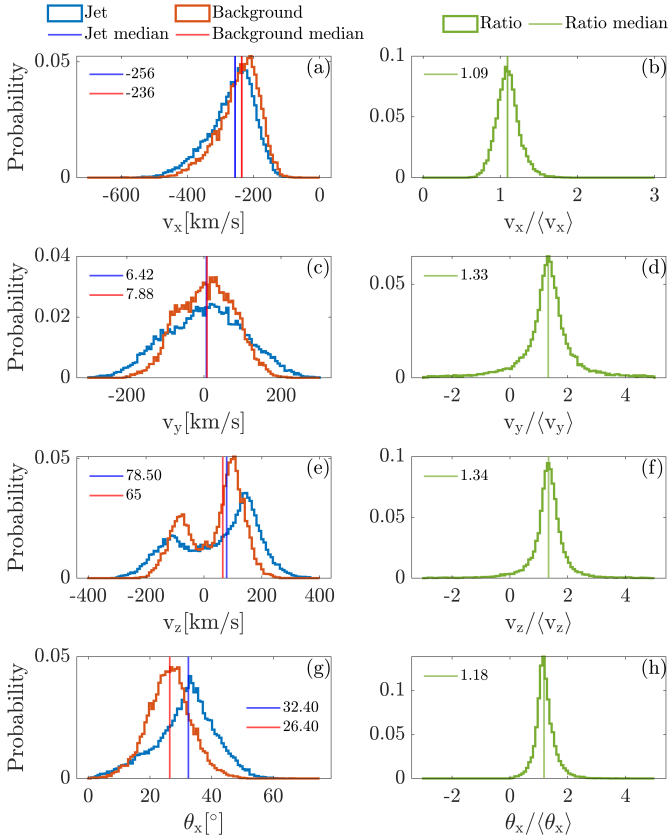

Fig. A.3. Same as Fig. 4, but for jets in the dayside magnetosheath.

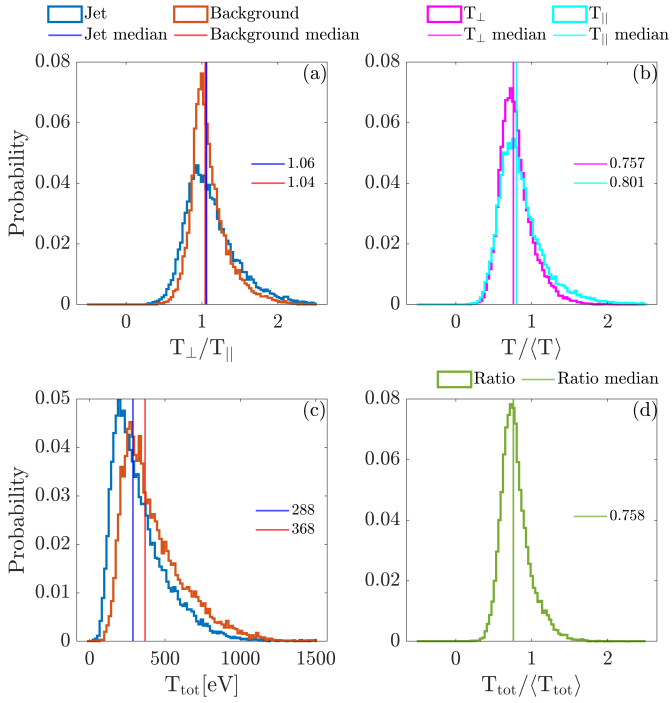

Fig. A.4. Same as Fig. 5, but for jets in the dayside magnetosheath.

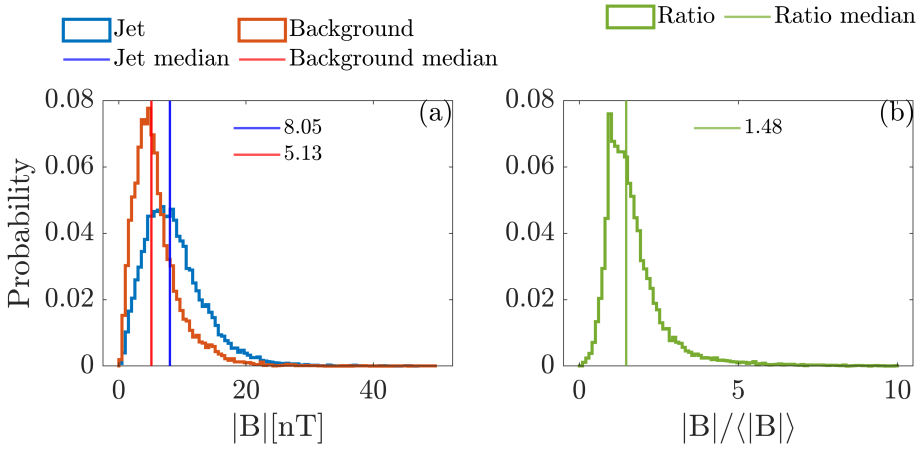

Fig. A.5. Same as Fig. 6, but for jets in the dayside magnetosheath.

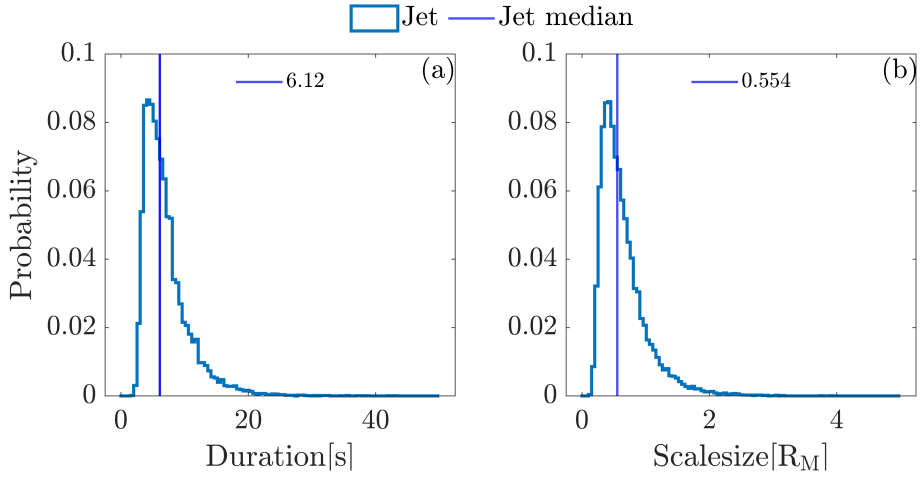

Fig. A.6. Same as Fig. 7, but for jets in the dayside magnetosheath.

Appendix B: Database statistics

In this appendix, we show statistics that are complementary to the data in Fig. 1 and in the main text. Figure B.1 shows the number of jets in each spatial bin in cylindrical coordinate in the entire database. Figure B.2 shows the cumulated duration the MAVEN spacecraft spent in each of those bins.

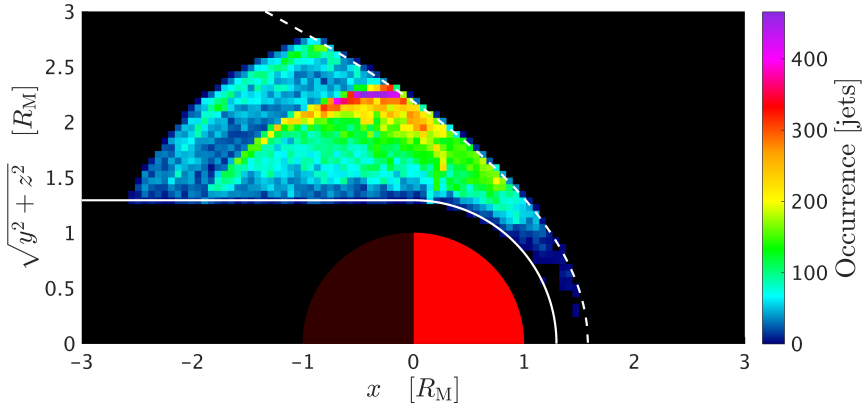

Fig. B.1. Number of jet observations in the Martian plasma environment in cylindrical coordinates. The solid white line represents the inner boundary of our dataset. The dashed white line represents the outer boundary, i.e. the average bow shock position.

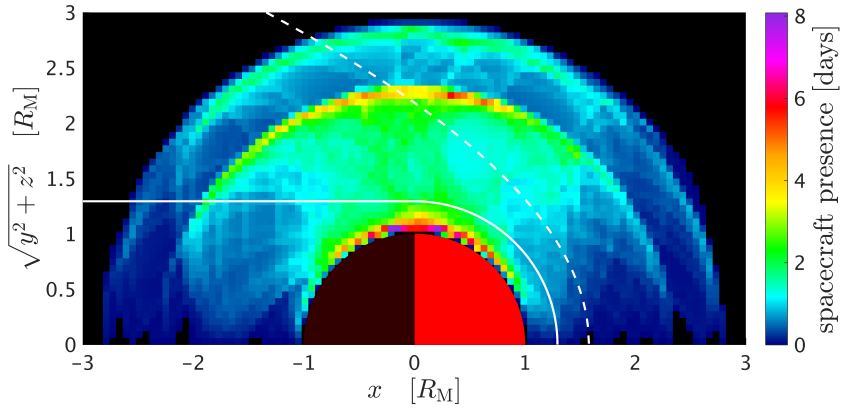

Fig. B.2. Spacecraft presence of the MAVEN spacecraft in cylindrical coordinates. The solid white line represent the inner boundary of our dataset. The dashed white line represents the outer boundary, i.e. the average bow shock position.